Journal of Hazardous Materials 163 (2009) 65–72

Contents lists available at ScienceDirect

Journal of Hazardous Materials

journal homepage: www.elsevier.com/locate/jhazmat

Uranium and thorium sequestration by a *Pseudomonas* sp.: Mechanism and chemical characterization

Sufia K. Kazy[a,1], S.F. D'Souza[b], Pinaki Sar[c,*,2]

[a] *Department of Agricultural and Food Engineering, Indian Institute of Technology, Kharagpur 721302, India*
[b] *Nuclear Agriculture and Biotechnology Division, Bhabha Atomic Research Centre, Mumbai 400085, India*
[c] *Department of Biotechnology, Indian Institute of Technology, Kharagpur 721302, India*

ARTICLE INFO

Article history:
Received 9 February 2008
Received in revised form 18 May 2008
Accepted 16 June 2008
Available online 27 June 2008

Keywords:
Pseudomonas
Uranium
Thorium
Biosorption mechanism
Bioremediation

ABSTRACT

The mechanism and chemical nature of uranium and thorium sequestration by a *Pseudomonas* strain was investigated by transmission electron microscopy, energy dispersive X-ray (EDX) analysis, FTIR spectroscopy and X-ray diffractometry. Atomic force microscopy (AFM) used in the tapping mode elucidated the morphological changes in bacterial cells following uranium and thorium binding. Transmission electron microscopy revealed intracellular sequestration of uranium and thorium throughout the cell cytoplasm with electron dense microprecipitations of accumulated metals. Energy dispersive X-ray analysis confirmed the cellular deposition of uranium and thorium. EDX and elemental analysis of sorption solution indicated the binding of uranium and thorium by the bacterial biomass via displacement of cellular potassium and calcium. The strong involvement of cellular phosphate, carboxyl and amide groups in radionuclide binding was ascertained by FTIR spectroscopy. X-ray powder diffraction (XRD) analyses confirmed cellular sequestration of crystalline uranium and thorium phosphates. Overall results indicate that a combined ion-exchange–complexation–microprecipitation mechanism could be involved in uranium and thorium sequestration by this bacterium. Atomic force microscopy and topography analysis revealed an undamaged cell surface with an increase in cell length, width and height following radionuclide accumulation. The arithmetic average roughness (R_a) and root mean square (RMS) roughness (R_q) values indicated an increase in surface roughness following uranium and thorium sequestration.

1. Introduction

Uranium mining and mineral processing for nuclear power and nuclear weapon production have resulted in the generation of significant amounts of radioactive wastes with tremendous environmental impact. Radionuclides like uranium and thorium are of particular concern due to their high toxicity and long half lives, thus they are considered as severe ecological and public health hazards [1,2]. Once released, environmental fate of these radionuclides is significantly controlled by microbial activity as natural microbial flora often executes fascinating mechanisms of interaction with such metallic pollutants, viz., reductive/enzymatic precipitation, solubilization, bioaccumulation/biosorption, etc., which ultimately determine their environmental mobility and toxicity [3]. Among the several microbial processes that determine the environmental fate of metallic toxicants, biosorptive accumulation of uranium and other radionuclides is of recent interest for the development of microbe based bioremediation strategies to clean up contaminated sites. The conventional remediation methods are highly expensive and ineffective particularly at low metal concentrations [3–7]. Biosorption based removal and recovery of strategic and precious metals is considered as a potential alternative and an economically attractive strategy offering advantages like low operating cost, minimum ratio of disposable chemical and/or biological sludge volume and high efficiency in detoxifying very dilute effluent [8]. Furthermore, biosorbent materials often have high metal loading capacity and in some cases are highly specific for certain elements of particular interest [9]. Considering the abundance and diversity of microorganisms in the natural domain, it is of immense importance to identify and characterize microbial strains with high metal accumulation capacity and specificity. Understanding and exploring potential of microbe–metal interaction have gained recent inter-

* Corresponding author. Tel.: +91 3222 283754; fax: +91 3222 277190.
E-mail address: sarpinaki@yahoo.com (P. Sar).
[1] Present address: Department of Civil and Environmental Engineering, Rice University, Houston, TX 77005, USA.
[2] Present address: Department of Biochemistry and Cell Biology, Rice University, Houston, TX 77005, USA.

0304-3894/$ – see front matter © 2008 Elsevier B.V. All rights reserved.
doi:10.1016/j.jhazmat.2008.06.076

est owing to their importance in various high end biotechnological applications like biosensor, biofuel cells and most promisingly in microbe mediated nanomaterial synthesis. Identifying the microbial ligands/cellular processes involved in metal sequestration has lead to the development of engineered organisms with various cell surface display that facilitate their applications as industrial catalysts, biosorbents, bioremediation, biofuel and biosensors [10]. Microbial synthesis of metal nanocrystals is another very promising aspect with immense importance in metal bioremediation and synthesis of nanoparticles for various applications [11].

In order to facilitate the microbe based immobilization of radionuclides/metals, which is considered to be the only alternative to protect ground water from eventual contamination; increased attention needs to be focused on deciphering the underlying mechanism of microbial radionuclide/metal sequestration [4,9,12]. Only a few reports are available on the mechanism of radionuclide (uranium and thorium) sequestration by bacteria and this is yet to be studied in more detail. A mechanistic understanding of uranium and thorium biosorption will help us to devise an effective and economically feasible biosorption process for the removal/separation of these elements. Such an understanding would also be useful in developing a microorganism-based removal/recovery system for the highly radioactive transuranic elements, namely, americium, plutonium and neptunium. Among the few reports on mechanism of uranium and thorium biosorption, Tsezos and Volesky have investigated U and Th biosorption by *Rhizopus* and indicated the sorption mechanism consists of at least three processes (coordination, adsorption and precipitation) [13,14]. A multi site surface complexation phenomenon governed by the formation of U-carboxyl and U–H-phosphoryl surface species has been reported for U sorption onto *Bacillus subtilis* by Fowle et al. [15]. Merroun et al. investigated the interactions of the cells and the S-layer of *B. sphaericus* JG-A12 with uranium by using transmission electron microscopy, energy dispersive X-ray analysis and extended X-ray absorption fluorescence spectroscopic methods [16] and indicated the role of phosphate and carboxyl groups in U binding.

Previous investigations by our group have shown that the *Pseudomonas* strain (MTCC 3087) has a high capacity for metabolism-independent accumulation of uranium (540 mg g^{-1} biomass dry wt.) and thorium (430 mg g^{-1} biomass dry wt.), and may find a potential application for the removal and recovery of such elements from effluents [17–19]. The bacterium exhibited a rapid removal of actinide ions with high affinity particularly at low metal ion concentrations, which is desirable for the development of any biosorption process. Such promising observations led us to investigate the mechanism of radionuclide sequestration by this bacterium. The present work was undertaken to decipher the possible mechanism and chemical nature of uranium and thorium accumulation by the *Pseudomonas* strain. The mechanism of radionuclide–bacteria interaction has been elucidated by employing several analytical techniques such as FTIR spectroscopy, energy dispersive X-ray analysis (EDX), X-ray diffraction analysis (XRD), transmission electron microscopy (TEM) and atomic force microscopy (AFM).

2. Materials and methods

2.1. Microorganism and growth conditions

The bacterial strain used in the present study was a *Pseudomonas* sp. (strain MTCC 3087) isolated from garden soil and maintained in Tris-minimal medium [9]. Mid growth phase cells grown in Tris-minimal medium were collected by centrifugation (12,000 × *g*, 30 min), washed thrice with distilled water, lyophilized and used for biosorption experiments.

2.2. Biosorption experiments

Except where otherwise described, for all biosorption experiments, 50 mg (dry wt.) of lyophilized biomass was contacted with 100 mL of a 100 mg uranium or thorium L^{-1} solution (as nitrate, $UO_2(NO_3)_2{\cdot}6H_2O$ or $Th(NO_3)_2{\cdot}5H_2O$, Merck, Germany). After 12 h of shaking at 150 rpm and 30 °C the biomass was separated by centrifugation (12,000 × *g*, 10 min) and supernatant used for metal (U/Th) estimation. The biomass pellet was washed and lyophilized for spectroscopic analysis. The initial pH of all metal solutions was adjusted to either pH 4.0 (Th) or pH 5.0 (U) by the addition of 1:0 M NaOH or 1:0 M HNO_3. In each set, samples without biomass were used as controls. Dissolved uranium and thorium were determined either by the arsenazo III method [17,18] or by inductively coupled plasma atomic spectrometry (ICP-AES). The biosorption equilibrium uptake (*q*, mg metal g^{-1} biomass dry wt.) for each sample was calculated according to the mass balance of metal ion expressed as

$$q = \frac{V(C_0 - C_e)}{M}$$

where *V* is the sample volume (L), C_0 the initial metal ion concentration (mg L^{-1}), C_e the equilibrium or final metal concentration (mg L^{-1}) and *M* the biomass dry weight (g).

2.3. Transmission electron microscopy (TEM)

Transmission electron microscopy of bacterial cells was done by using the methodology as described previously [20]. Metal-free (control) and metal-loaded biomass obtained following centrifugation of sorption solution (biomass + metal solution) were washed thoroughly with sodium phosphate buffer (0.1 M, pH 7.2), fixed for 2 h at room temperature in 2.5% glutaraldehyde in the same buffer, followed by osmium tetraoxide staining (1%, 1 h). Cells were dehydrated via a graded ethanol series, treated with propylene oxide and embedded in epoxy resin. Unstained ultra thin sections were cut by a Reichert Ultracut E Ultramicrotome (Reichart, Germany), loaded on a formvar carbon-coated grid and examined in a Philips CM10 transmission electron microscope at 100 kV.

2.4. Energy dispersive X-ray microanalysis (EDX)

Metal-free control and metal-loaded lyophilized biomass were used for energy dispersive X-ray microanalysis using an OXFORD ISIS-300 microanalytical system attached with JEOL JSM-5800 Scanning electron microscope.

2.5. Elemental (K and Ca) analysis

Analysis of K and Ca content of the supernatant of metal-free biomass solution or of metal-biomass sorption solution was done using Flame Photometer (Flame Photometer, 128, Systronics, India).

2.6. FTIR spectroscopy

Metal-free control and metal-loaded lyophilized biomass were used for FTIR spectroscopic analysis. The infrared spectra were recorded within the range 400–4000 cm^{-1} in a Thermo Nicolet NEXUS-870 FTIR Spectrometer.

2.7. X-ray powder diffraction analysis (XRD)

X-ray diffraction pattern of lyophilized powder samples of metal-free control and metal-sorbed biomass was recorded in a Philips X'Pert Pro Panalytical PW3040/60 powder diffractometer

using Co source radiation ($\lambda = 1.79$) over the range of 0–100 (2θ) with a step length of 0.05° and time per step 29.8 s. The chemical nature of U/Th crystals was determined based on comparison with the powder diffraction standard files (Search Manual for Selected Powder Diffraction Data for Metals and Alloys, JCPDS, International Centre for Diffraction Data, PA, USA, 1978).

2.8. Atomic force microscopy (AFM)

Uranium/thorium exposed bacterial cells recovered by centrifugation were mounted on glass slides, air dried (22–28 °C) and used for atomic force microscopy. Specimens were viewed using a SPM 100 Atomic force microscope (Nanonics Imaging Ltd., Israel). Imaging was carried out using microfabricated glass tips with a spring constant of 5 N m^{-1}, tip radius 20 nm, in intermittent contact mode.

All data represent the mean of three independent experiments. Standard deviations and error bars are indicated wherever necessary. All statistical analyses were done using Microcal™ Origin, Version 6.0.

3. Results and discussion

3.1. Transmission electron microscopy and energy dispersive X-ray microanalysis

Pseudomonas cells before and after metal (U and Th) exposure (100 mg L^{-1}, 12 h), were subjected to transmission electron microscopy to ascertain the cellular localization of accumulated metals (Fig. 1). Ultra thin sections of metal less control cells revealed a distinct cell boundary and clear cytoplasm with few electron dense areas probably representing the genetic material and cytoplasmic deposits. In contrast to this, metal-loaded cells exhibited dark electron opaque region through out the cytoplasm with few electron dense deposits around cell boundary and cell interior indicating homogeneous intracellular sequestration of accumulated U/Th. Few granular deposits observed near cell wall and cytoplasmic region could be attributed to the microprecipitation of crystalline U/Th phosphates as also confirmed later by X-ray diffraction analyses. Noticeably, for both U and Th loaded cells, with blacked cytoplasm no structural damage or distortion of the cells is apparent.

Conclusive identification of the deposited element was achieved by energy dispersive X-ray microanalysis (EDX) (Fig. 2). Compared to the metal-free control samples, presence of specific peaks for uranium and thorium in respective U- and Th-loaded samples confirmed the presence of accumulated radionuclides. The electron microscopy and EDX studies, although essentially qualitative in nature, suggest that the major site of uranium and thorium deposition is the cell cytoplasm. Studies on microbial accumulation of actinide elements including uranium and other heavy metals have indicated a selective sequestration of accumulated metals in different parts of the microbial cell. In many cases of enzymatic metal sequestration (including U) by dissimilatory iron reducing (*Geobacter*, *Desulfovibrio*, etc.) or by metal resistant bacteria (*Citrobacter*, *Pseudomonas* and *Escherichia coli*) and even in metabolism-independent biosorption process, the sequestered metal was found to be localized in and around cell boundary (outer membrane, LPS, EPS, periplasm). Compared to uranium, information on cellular localization of thorium is relatively scanty. Gadd and White had demonstrated cytosolic Th accumulation by *Saccharomyces cerevisiae* irrespective of their growth phase [21]. In case of *Rhizopus arrhizus*, non-metabolizing cells were found to sequester accumulated Th in the cell wall [14].

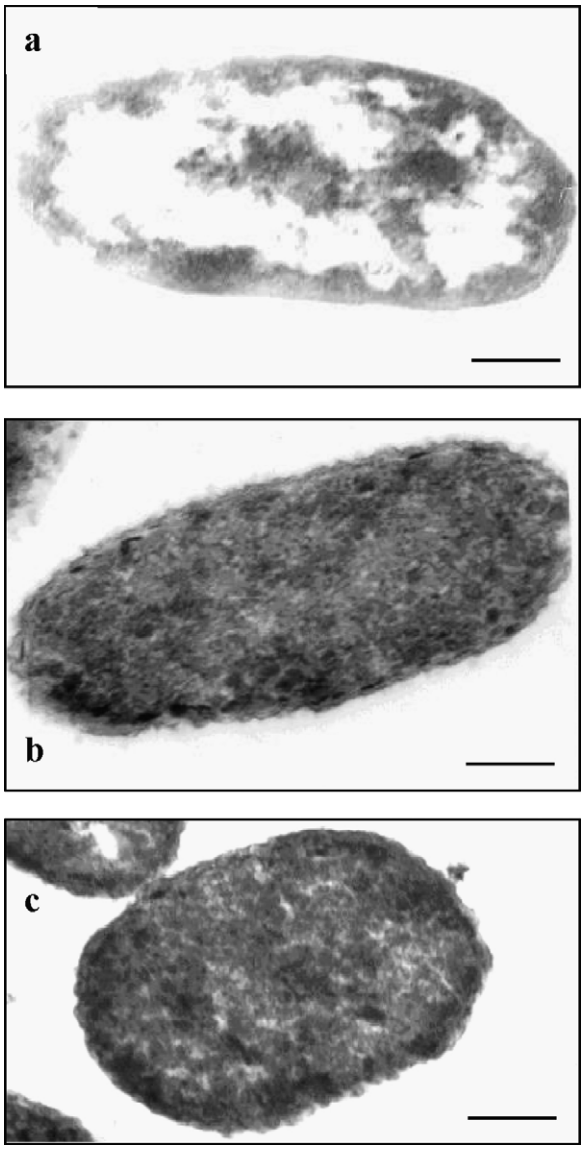

Fig. 1. Transmission electron micrographs of *Pseudomonas* sp.: before (a) and after uranium (b) and thorium (c) accumulation. Bar indicates 200 nm.

Unlike previous reports on peripheral deposition of uranium in the cell wall region [22], which is largely due to the inability of uranyl ions to enter the cytoplasmic compartment of living cells resulting from the large size and stereochemistry of UO_2^{2+} and its associated hydroxyl groups [23], intracellular uranium and thorium deposition as observed in the present study corroborate well with previous reports on intracellular uranium accumulation by *P. aeruginosa* and other bacterial strains [23,24]. Such metabolism-independent intracellular radionuclide sequestration may be attributed to non-specific transport due to increased membrane permeability, resulting from toxicity in living cells. Regarding the stoichiometry of radionuclide binding, the test bacterial cells showed intracellular deposition of thorium and uranium amounting to 43–54% of cell dry weight [17,18], and with almost all cells exhibiting intracellular metal accumulation, it is difficult to imagine that there are sufficient binding sites to account for this much metal loading. Such non-stoichiometric accumulation of metals by bacterial cells or cell wall components were also previously reported and could be ascribed to the fact that metal ion complex with existing reactive sites and that additional metal crystallization on these

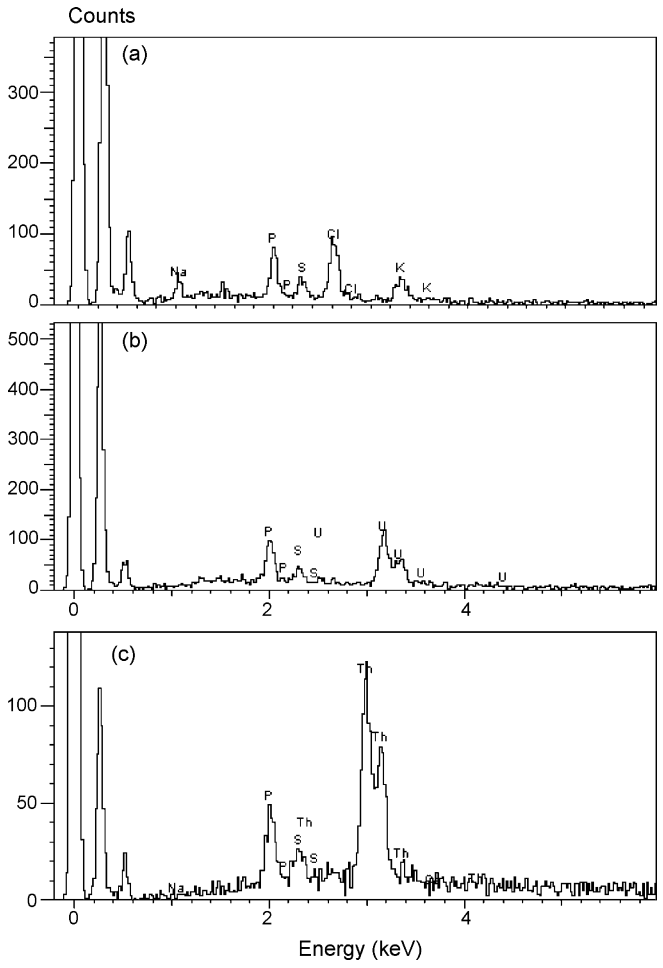

Fig. 2. Energy dispersive X-ray analyses of *Pseudomonas* sp. biomass: before (a) and after uranium (b) and thorium (c) accumulation.

bound molecules facilitates excess metal loading [24,25]. Microprecipitation of accumulated metals may also be resulted in metal sequestration several folds of cellular dry weight [8].

Energy dispersive X-ray microanalysis was employed to estimate the elemental content of the biomass sample. This bulk technique gives an elemental ratio of the population as a whole, analyzing the whole pellet following metal exposure. The lyophilized bacterial biomass was subjected to EDX analysis before and after metal (uranium and thorium) accumulation. The EDX spectrum of the biomass before metal uptake (Fig. 2a) exhibited distinct peaks of phosphorous, potassium and sulphur indicating the substantial presence of these elements in the biomass. Following metal (U or Th) uptake, the spectra (Fig. 2b and c) showed distinct peaks for respective metals (U or Th), but no peak for potassium. This observation is supported further by determining relative abundance values of Ca and K, obtained from the microanalysis of elements present in the U- and Th-exposed samples (K, not detected; Ca, insignificant concentration (<2 sigma) compared to the unexposed (control) biomass (K, 18.5% and Ca, 1.64%). To check the possible release of cellular potassium (K) and calcium (Ca), following radionuclide sorption, elemental analysis of the sorption solution was performed after the sorption process was over. Compared to the metal-free biomass solution (control), the U/Th-biomass sorption solution showed the presence of substantial amounts of K (6.5 and 6.8 mg L^{-1} in U and Th sorption solution, respectively) and Ca (1.7 and 1.9 mg L^{-1} in U and Th sorption solution, respectively), clearly indicating the release of these ions from the biomass following U and Th sorption. Concomitant with metal uptake, ion (K, Ca, Mg, Na, or H) release from the biomass is a frequently observed event that has significance in deciphering the mechanism of metal biosorption. It has been suggested that ion exchange rather than sorption to free sites could be a relevant mechanism for the binding of metal ions on to the biomass; since the charge of the biomass particle has to be neutral, any binding of one cation must be accompanied by either stoichiometric release of other cations or by the binding of anions [8]. Several previous reports have demonstrated extensive K release from biomass following metal uptake suggesting K release to maintain ionic balance across the membrane. The observed replacement of K^+ and Ca^{2+} by U/Th ions may further be analyzed in light of the fact that potassium and calcium are hard cations, bind O- and P-donor ligands with low affinity ionic bonds. On the other hand, uranium and thorium are soft ions; bind O- and P-donor ligands strongly. The overall observation from the present data strongly indicates the possibility of uranium and thorium binding with the biomass by displacing cellular potassium through ion-exchange mechanism.

3.2. X-ray powder diffraction (XRD) analysis

To elucidate the chemical nature of bacterial cell bound radionuclides, test biomass was subjected to X-ray diffraction analysis before (control) and after uranium or thorium sequestration (Fig. 3). In contrast to untreated control biomass, which is an expectedly amorphous, XRD spectrum for biomass loaded with uranium and thorium showed distinct reproducible patterns typical for the presence of well-crystallized materials. Following uranium accumulation, the XRD pattern of bacterial biomass showed two distinct peaks at 2θ 7.66° and 6.36°. Comparison of respective *d*-spacing values of 5.324 and 6.412 Å with data files of known compounds (JCPDS), showed satisfactory correlation with the lines of uranium phosphate compounds ($U_3(PO_4)$, $U(UO_2)_3(PO_4)_2(OH)_6{\cdot}4H_2O$, $U(UO_2)_3(PO_4)_2(OH)_6{\cdot}2H_2O$) (Characteristic lines at 6.46, 5.30 and 5.38 Å, with 50% or more intensity). Similar to this, Th loaded biomass also showed two distinct peaks at 2θ 6.64° and 7.94° corresponding to *d*-spacing values of 6.142 and 5.137 Å. Based on d spacing values these peaks are attributed to the presence of crystalline thorium phosphates ($Na_2ThP_2O_8$ and $Th_3(PO_3)_4$) (characteristic lines at 6.14, 5.18 and 5.10 Å, with 100% intensity for the former). The crystalline uranium and thorium phosphate formation following actinide accumulation indicate possible complexation of such metals with the cellular phosphate groups facilitating metal nucleation and metal precipitation in a crystalline state [8,9]. FTIR spectroscopic analysis of the test biomass also indicated involvement of cellular phosphate groups in uranium and thorium binding as described above. Phosphate groups may be available from intracellular phosphates, while phosphonate groups and phospholipids from cell membrane and wall materials may act as the primary metal binding sites creating negative surface charge conductive to cation binding [26,27]. Implication of these groups in the complexation of uranium in Gram-negative bacteria is previously confirmed using different spectroscopic and microscopic techniques [16]. The initial binding of metal ions to biomass reactive sites may serve as nucleation sites for further precipitation of metals forming large metal deposits [8]. Formation of crystalline uranium phosphates by different bacterial strains has been observed previously [3,28,29], where as sequestration of crystalline thorium phosphate is relatively unreported except the report of thorium phosphate formation by *Citrobacter*, in presence of lanthanum and organic phosphate donor [30].

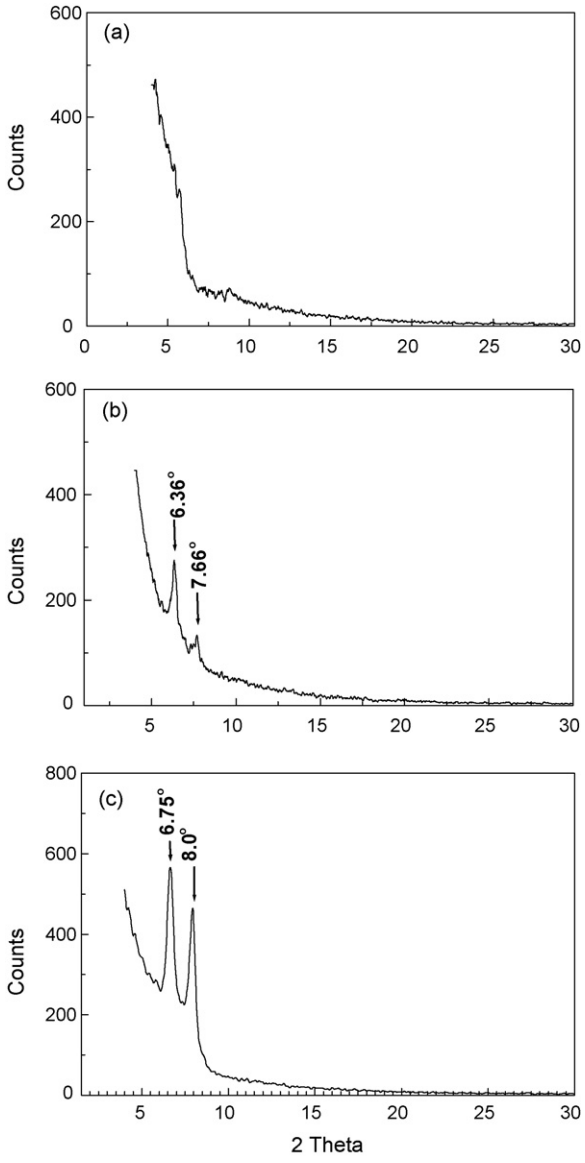

Fig. 3. X-ray powder diffraction analyses of *Pseudomonas* sp. biomass: before (a) and after uranium (b) and thorium (c) accumulation.

3.3. FTIR spectroscopy

FTIR spectroscopies for control (metal-free) and for uranium and thorium loaded biomass were recorded to elucidate the chemical groups involved in metal (U/Th) binding on to the bacterial biomass (Fig. 4). Analyzing the highly complex IR spectra, certain characteristic peaks can be assigned to the involvement of the main functional groups present in the bacterial biomass. The spectrum of the native biomass showed a characteristic peak in the 3787 cm^{-1} region due to the stretching of the O–H bond of carboxylic acids present in the biomass [31]. In the spectrum of U-loaded cells, this peak was shifted to the 3784 cm^{-1} region, which is attributable to the role of carboxylic acid in uranium binding. In the control spectrum, a peak in the 3500–3200 cm^{-1} region is due to the stretching of the N–H bond of amino groups. This N–H stretching peak lies in the spectrum region occupied by a broad and strong band (3200–3600 cm^{-1}), which is due to the presence of γO–H of the hydroxyl groups [32]. A change in peak position in the spectrum of both U- and Th-loaded samples indicate the binding of such metals with amino and hydroxyl groups. In the control spectrum, the complex absorption at 2900–3000 cm^{-1} are ascribed to the asymmetric stretching of γC–H bond of $-CH_2$ groups combined with that of the CH_3 groups [33]. All three spectra for the bacterial samples, with or without radionuclide binding, revealed presence of protein related bands. The γC=O of amide I and δNH/γC=O combination of the amide II bonds were prominent at ~1665 and 1545 cm^{-1}, respectively. The principle amide I absorption peak at 1665 cm^{-1} is mainly accounted for by the 3_{10}-helical structure of proteins, although, amino sugars (with *N*-acetyl/glucuronamide groups) also have a strong absorbance in that region [33]. Compared to metal-free control cells, the spectra for uranium and thorium accumulated samples showed a minor shift in the position of the 1665 cm^{-1} peak to 1666 cm^{-1} and to 1663 cm^{-1}, respectively. The intense amide II bands that come in the range of 1520–1550 cm^{-1}, presented a significant change after uranium and thorium binding. Although variation in the energies and intensities of these bands are minor, the intensity ratio of amide I to amide II decreased (30%) following U/Th sorption. The observed changes in peak positions and relative intensities, most likely reflect some alteration in the secondary structure of cellular proteins from the dominating 3_{10}-helix (1665 cm^{-1}) to other possible conformation as a result of radionuclide sequestration. In the control spectrum the sharp peaks in between 1400 and 1500 cm^{-1} region are due to the presence of carboxyl groups [34]. Following U and Th sorption, the spectra exhibited changes in peak positions further indicating the strong role of carboxyl groups in radionuclide binding. In the control, the strong peaks in the 1241 and 1072 cm^{-1} region are attributable to the presence of both carboxyl and phosphate groups, respectively. Following metal sorption, a clear shift of these peaks indicates the strong interaction of U and Th with these groups [26,27]. The

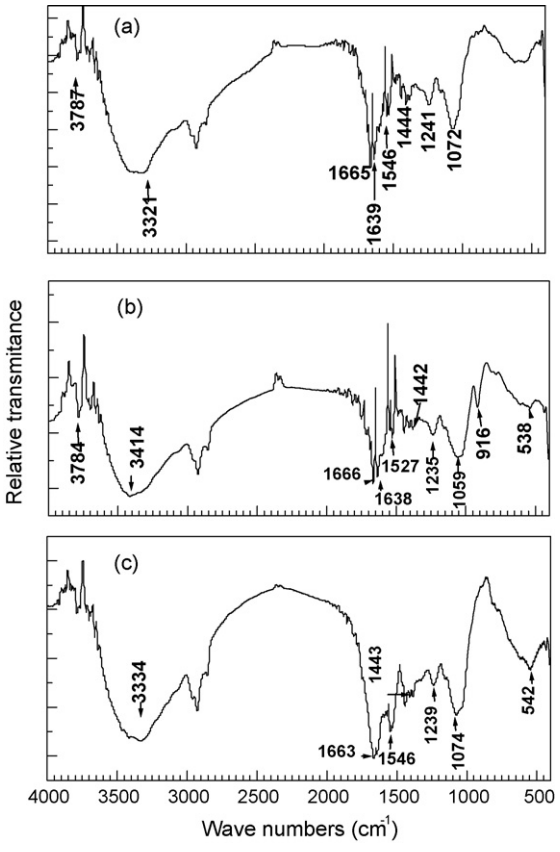

Fig. 4. Fourier transformed IR spectra of *Pseudomonas* sp. biomass: before (a) and after uranium (b) and thorium (c) accumulation.

asymmetric stretching modes of protonated polyphosphates and $PO_{uncomplexed}$ in phosphate diesters have been shown to absorb strongly around 1240 cm^{-1} [35]. A decrease in intensity and a gradual shift of the peak at 1241 cm^{-1}, in the control sample to a lower energy in uranium (1235 cm^{-1}) and thorium (1239 cm^{-1}) loaded samples clearly indicates the weakening of the P=O character as a result of radionuclide binding to the phosphates. The strong absorption peaks in between 1000 and 1100 cm^{-1} also ascertained the presence of carboxyl groups in the bacterial polysaccharide structure and after metal binding by the biomass, a prominent change in peak positions (1072–1059 cm^{-1} for uranium loaded biomass and 1072–1074 cm^{-1} for thorium loaded biomass) in this region strongly suggest the involvement of carboxyl groups in U and Th sorption [34]. An obvious change in the peak position and intensity at 800–400 cm^{-1} region could be assigned to the formation of intense δ(M–O) and δ(O–M–O) bonds (M = metal ion) [9]. In the uranium loaded sample, the distinct peak at 916.7 cm^{-1} and changes in peak positions and intensity around 550–1000 cm^{-1} region can be assigned to asymmetric stretching vibration of ν_3 UO_2^{2+} and stretching vibrations of weekly bonded oxygen ligands with uranium (ν U–O_{ligand}) [36]. The overall spectral analysis strongly supports the major role of carboxyl and phosphate groups in uranium and thorium binding by the bacterial biomass. A previous report on EXAFS analysis of the uranium bound to the bacterial surface protein indicated that sequestered U is coordinated by phosphate groups in a monodentate mode and by carboxyl groups in a bidentate fashion [16].

3.4. Atomic force microscopy

The atomic force microscope (AFM) is an ideal tool for determining changes in cellular morphology. In the present study AFM was used to investigate the bacterial cell surface morphology following uranium and thorium sorption. AFM imaging was performed using the tapping mode, where, the tip makes intermittent contact with the sample as the tip is oscillated near its resonance frequency. The advantages of the tapping mode are that the sample is less likely to be damaged by the tip and that lateral forces are greatly reduced [37]. Despite these advantages, there are very few reports on application of this technique in investigating bacterial metal/radionuclide sequestration processes.

As it was difficult to resolve images with fresh hydrated cells, air dried cells on glass cover slips were used for morphological comparison among the cells before and after radionuclide sorption (Fig. 5). Both metal-free control cells and cells after U/Th sorption formed a patched layer on the glass surface and individual cells can be identified very well. Although the preparation technique used did not give a monolayer of cells, the bacterial cells are distinguishable in AFM images. Most of the bacterial cells are found packed close to one another forming compact covering. AFM line analyses of the cells shown in Fig. 5 are presented in Table 1. Topography analyses of the cells before and after uranium and thorium sorption revealed undamaged cell surface with variation in cell size. It is clear that following metal sorption, there is an increase in cell length, width and height. Noticeably, this enhancement in cell length and height is more with thorium (L: 1.6-fold, H: 1.74) compared to uranium treated cells (L: 1.21, H: 1.30). The latter cells, however, showed a greater increase in width (2.02-fold) compared to that of thorium loaded cells. The arithmetic average roughness R_a and root mean square (RMS) roughness R_q values further revealed an increase in surface roughness following uranium (×2.78-fold) and thorium (×1.67-fold) sorption. Overall results indicate that surfaces were rougher or irregular following uranium and thorium binding. Surface roughness of bacterial cells also have been observed previously and quantified using AFM, however, reports on the effect of radionuclides on the bacterial cell surface is scanty. Previous report on atomic force microscopy studies reveals that lanthanum binding to *E. coli* substantially changes the structure of the outer cell membrane responsible for the cell permeability [38]. Wang et al. have reported a similar change in cell dimensions and roughness following metallization of nickel

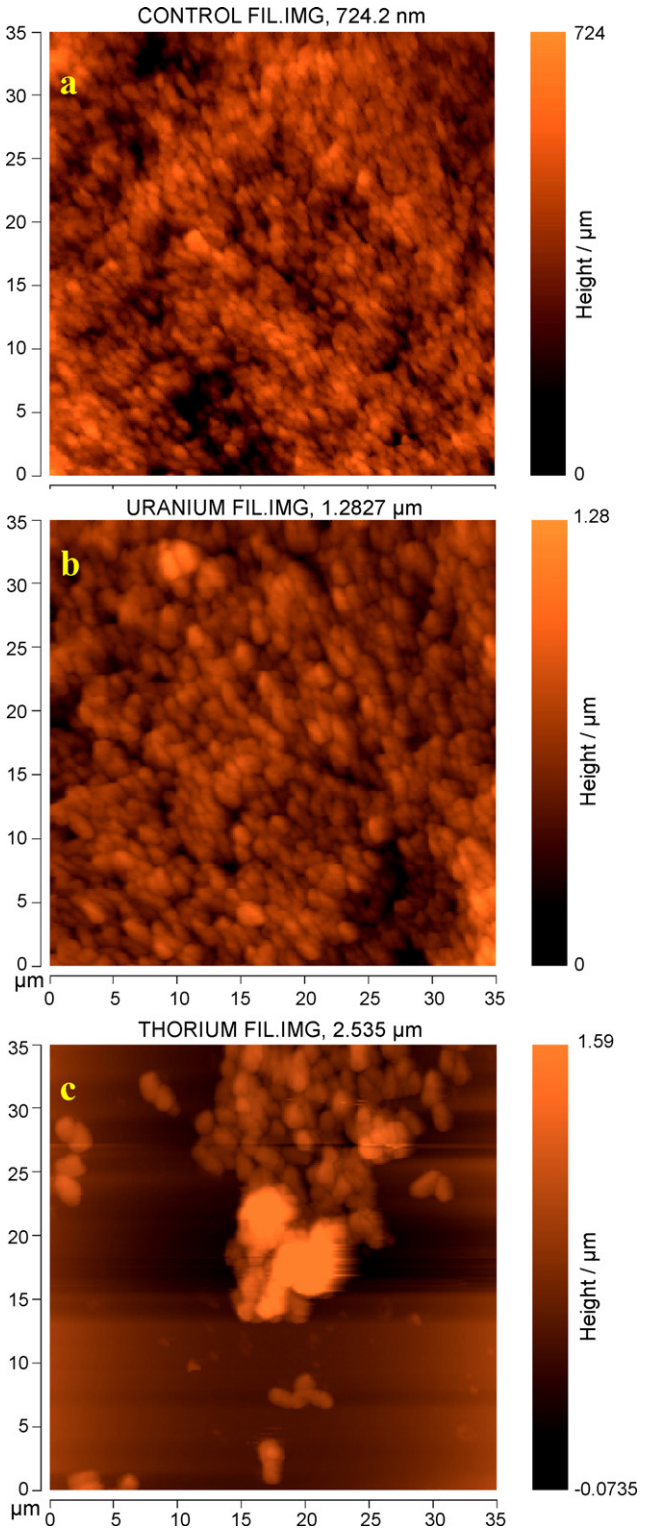

Fig. 5. Atomic force microscopic images of bacterial cells before (a) and after uranium (b) and thorium (c) accumulation.

Table 1
Effect of uranium and thorium sequestration on bacterial cell dimensions[a] and surface roughness

	Cell length (nm)	Width (nm)	Height (nm)	Roughness (nm)	
				R_a	R_q (RMS)
Control	1724 ± 80	689 ± 20	458 ± 23	32.28 ± 1.5	37.15 ± 0.87
U	2093 ± 83	1395 ± 56	635 ± 28	92.96 ± 3.6	103.06 ± 3.1
Th	2762 ± 133	1242 ± 55	797 ± 32	56.59 ± 2.5	62.04 ± 2.5

[a] Cell dimensions were determined from topography analysis of AFM images.

by *E. coli* cells [39]. Cell surface properties in gm negative bacteria (including *Pseudomonas*) are strongly regulated by surface proteins and lipopolysaccharides. Interaction of radionuclides (uranium and thorium) with such macromolecules with strong metal binding ligands (phosphate and carboxyl), possibly leads to a change in surface architecture as reflected by an increase in surface roughness. Another reason of increased roughness is possible rupturing of the bacterial cell following U/Th accumulation, which was reported by earlier workers characterizing *Pseudomonas* cells following U and Pt accumulation [40].

4. Conclusion

The present work delineates the chemical nature of bacteria–radionuclide interaction with a mechanistic approach. Intracellular radionuclide (uranium and thorium) deposition is observed through transmission electron microscopy that also reveals presence of electron dense microprecipitation of deposited metals. Elemental analysis of biomass and uptake solution indicated that uranium and thorium binding by the bacterial cells is possibly mediated by displacement of cellular potassium and calcium ions. Involvement of cellular phosphate, carboxyl and amide groups in uranium and thorium binding is evident from FTIR spectroscopy. Role of cellular phosphate groups in uranium and thorium sequestration is confirmed by X-ray powder diffraction analyses that showed deposition of crystalline uranium and thorium phosphate within the cell biomass. Atomic force microscopy showed enlargement of bacterial cells following radionuclide sorption along with increase in surface roughness.

The overall observations suggest that the high uranium and thorium accumulation by the test bacterium could be due to the result of a combined ion-exchange–complexation–microprecipitation mechanism, which is a new report for uranium and thorium biosorption by metabolically inactivated bacterial cells. This report strengthen the concept that combination of several mechanisms, such as adsorption, ion-exchange, complexation, coordination, chelation or microprecipitation, each functioning independently, can contribute to the overall metal accumulation in biosorption.

Acknowledgements

Sufia K Kazy gratefully acknowledges the financial assistance received from Council of Scientific and Industrial Research (CSIR), India. Pinaki Sar acknowledges the financial assistance received from Department of Science and Technology, India for Fast Track project and Department of Atomic Energy, India for DAE Young Scientist project.

References

[1] I. Hore-Lacy, C.J. Cleveland, Naturally-occurring radioactive materials (NORM), in: C.J. Cleveland (Ed.), Encyclopedia of Earth, Environmental Information Coalition, National Council for Science and the Environment, Washington, DC, 2006.
[2] J.R. Lloyd, J.C. Renshaw, Bioremediation of radioactive waste: radionuclide–microbe interactions in laboratory and field-scale studies, Curr. Opin. Biotechnol. 16 (2005) 254–260.
[3] J.R. Lloyd, L.E. Macaskie, Bioremediation of radionuclide containing wastewaters, in: D.R. Loveley (Ed.), Environmental Metal Microbe Interaction, American Society of Microbiology, Washington, DC, 2000, pp. 277–327.
[4] H.H. Tabak, P. Lens, E.D. van Hullebusch, W. Dejonghe, Developments in bioremediation of soils and sediments polluted with metals and radionuclides: microbial processes and mechanisms affecting bioremediation of metal contamination and influencing metal toxicity and transport, Rev. Environ. Sci. Biotechnol. 4 (2005) 115–156.
[5] S. Xie, J. Yang, C. Chen, X. Zhang, Q. Wang, C. Zhang, Study on biosorption kinetics and thermodynamics of uranium by *Citrobacter freudii*, J. Environ. Radioactivity 99 (2008) 126–133.
[6] M.H. Khani, A.R. Keshtkar, M. Ghanadi, H. Pahlavanzadeh, Equilibrium, kinetic and thermodynamic study of the biosorption of uranium onto *Cystoseria indica* algae, J. Hazard. Mater. 150 (2008) 612–618.
[7] K. Akhtar, W. Akhtar, A.M. Khalid, Removal and recovery of uranium from aqueous solutions by *Trichoderma harzianum*, Water Res. 41 (2007) 1366–1378.
[8] B. Volesky, S. Schiewer, Biosorption metals, in: M.C. Flickinger, S.W. Drew (Eds.), Encyclopedia of Bioprocess Technology: Fermentation, Biocatalysis and Bioseparation, John Wiley and Sons, New York, 2000, pp. 433–453.
[9] S.K. Kazy, S.K. Das, P. Sar, Lanthanum biosorption by a *Pseudomonas* sp.: equilibrium studies and chemical characterization, J. Ind. Microbiol. Biotechnol. 33 (2006) 773–783.
[10] D. Mandal, M.E. Bolander, D. Mukhopadhyay, G. Sarkar, P. Mukherjee, The use of microorganisms for the formation of metal nanoparticles and their application, Appl. Microbiol. Biotechnol. 69 (2006) 485–492.
[11] C.H. Wu, A. Mulchandani, W. Chen, Versatile microbial surface display for environmental remediation and biofuels production, Trends Microbiol. 16 (2008) 181–188.
[12] T. Barkay, J. Schaefer, Metal and radionuclide bioremediation: issues, considerations and potentials, Curr. Opin. Microbiol. 4 (2001) 318–323.
[13] M. Tsezos, Biosorption of Uranium and Thorium, McGill University, Montreal, 1980.
[14] M. Tsezos, B. Volesky, The mechanism of thorium biosorption by *Rhizopus arrhizus*, Biotechnol. Bioeng. 24 (1982) 955–969.
[15] D.A. Fowle, J.B. Fein, A.M. Martin, Experimental study of uranyl adsorption on to *Bacillus subtilis*, Environ. Sci. Technol. 34 (2000) 3737–3741.
[16] M.L. Merroun, J. Raff, A. Rossberg, C. Hennig, T. Reich, S. Selenska-Pobell, Complexation of uranium by cells and S-layer sheets of *Bacillus sphaericus* JG-A12, Appl. Environ. Microbiol. 71 (2005) 5532–5543.
[17] P. Sar, S.F. D'Souza, Biosorptive uranium uptake by a *Pseudomonas* strain: characterization and equilibrium studies, J. Chem. Technol. Biotechnol. 76 (2001) 1286–1294.
[18] P. Sar, S.F. D'Souza, Biosorption of thorium by a Pseudomonas biomass, Biotechnol. Lett. 24 (2002) 239–243.
[19] S.F. D'Souza, P. Sar, S.K. Kazy, B.S. Kubal, Uranium sorption by Pseudomonas biomass immobilized in radiation polymerized polyacrylamide bio-beads, J. Environ. Sci. Health A Tox Hazard Subst. Environ. Eng. 41 (2006) 487–500.
[20] P. Sar, S.K. Kazy, S.P. Singh, Intracellular nickel accumulation by *Pseudomonas aeruginosa* and its chemical nature, Lett. Appl. Microbiol. 32 (2001) 257–261.
[21] G.M. Gadd, C. White, Uptake and intracellular compartmentation of thorium in *Saccharomyces cerevisiae*, Environ. Poll. 61 (1989) 187–197.
[22] Y. Suzuki, J.F. Banfield, Geomicrobiology of uranium, in: P.C. Burns, R. Finch (Eds.), Uranium: Mineralogy, Geochemistry and the Environment, Mineralogical Society of America, Washington, DC, 1999, pp. 393–432.
[23] B.C. Jeong, C. Hawes, K.M. Bonthrone, L.E. Macaskie, Localization of enzymically enhanced heavy metal accumulation by *Citrobacter* sp. and metal accumulation in vitro by liposome containing entrapped enzyme, Microbiology 143 (1997) 2497–2507.
[24] G.W. Strandberg, S.E. Shumate, J.R. Parrot, Microbial cells as biosorbents for heavy metals: accumulation of uranium by *Saccharomyces cerevisiae* and *Pseudomonas aeruginosa*, Appl. Environ. Microbiol. 41 (1981) 237–245.
[25] T.J. Beveridge, The response of cell walls of *Bacillus subtilis* to metals and to electron-microscopic stains, Can. J. Microbiol. 24 (1978) 89–104.
[26] M.L. Merroun, K.B. Chekroun, J.M. Arias, M.T. González-Muñoz, Lanthanum fixation by *Myxococcus xanthus*: cellular location and extracellular polysaccharide observation, Chemosphere 52 (2003) 113–120.
[27] M.L. Merroun, G. Geipel, R. Nicolai, K.H. Heise, S. Selenska-Pobell, Complexation of uranium (VI) by three eco-types of *Acidithiobacillus ferrooxidans* studied using time-resolved laser-induced fluorescence spectroscopy and infrared spectroscopy, BioMetals 16 (2003) 331–339.
[28] Y. Andres, H.J. MacCordick, J.C. Hubert, Selective biosorption of thorium ions by an immobilized mycobacterial biomass, Appl. Microbiol. Biotechnol. 44 (1995) 271–276.
[29] M.J. Beazley, R.J. Martinez, P.A. Sobecky, S.M. Webb, M. Taillefert, Uranium biomineralization as a result of bacterial phosphatase activity: insights from bacterial isolates from a contaminated subsurface, Environ. Sci. Technol. 41 (2007) 5701–5707.
[30] P. Yong, L.E. Macaskie, Bioaccumulation of lanthanum, uranium and thorium, and use of a model system to develop a method for biologically mediated removal of plutonium from solution, J. Chem. Technol. Biotechnol. 71 (1998) 15–26.

[31] P.X. Sheng, Y.P. Ting, J.P. Chen, L. Hong, Sorption of lead, copper, cadmium, zinc and nickel by marine algal biomass, J. Colloid Interface 275 (2004) 131–141.
[32] F. Pagnanelli, P.M. Petrangeli, L. Toro, M. Trifoni, F. Veglio, Biosorption of metal ions on *Arthrobacter* sp.: biomass characterization and biosorption modeling, Environ. Sci. Technol. 34 (2000) 2773–2778.
[33] I. Beech, L. Hanjagsit, M. Kalaji, A.L. Neal, V. Zinkevich, Chemical and structural characterization of exopolymers produced by *Pseudomonas* sp. NCIMB 2021 in continuous culture, Microbiology 145 (1999) 1491–1497.
[34] S.K. Kazy, P. Sar, A.K. Sen, S.P. Singh, S.F. D'Souza, Extracellular polysaccharides of a copper-sensitive and a copper-resistant *Pseudomonas aeruginosa* strain: synthesis, chemical nature and copper binding, W, J. Microbiol. Biotechnol. 18 (2002) 583–588.
[35] W. Jiang, A. Saxena, B. Song, B.B. Ward, T.J. Beveridge, S.C.B. Myneni, Elucidation of functional groups on Gram-positive and Gram-negative bacterial surfaces using infrared spectroscopy, Langmuir 20 (2004) 11433–11442.
[36] J. Cejka, Infrared spectroscopy and thermal analysis of the uranyl minerals, in: P.C. Burns, R. Finch (Eds.), Uranium: Mineralogy, Geochemistry and the Environment, Mineralogical Society of America, Washington, DC, 1999, pp. 521–622.
[37] T.A. Camesano, M.J. Natan, B.E. Logan, Observation of changes in bacterial cell morphology using tapping mode atomic force microscopy, Langmuir 16 (2000) 4563–4572.
[38] L. Peng, L. Yi, L. Zhexue, Z. Juncheng, D. Jiaxin, P. Daiwen, S. Ping, Q. Songsheng, Study on biological effect of La^{3+} on *Escherichia coli* by atomic force microscopy, J. Inorg. Biochem. 98 (2004) 68–72.
[39] J. Wang, S. He, X.U. Lina, G.U. Ning, Transmission electron microscopy and atomic force microscopy characterization of nickel deposition on bacterial cells, Chin. Sci. Bull. 52 (2007) 2919–2924.
[40] S. Krueger, G.J. Olson, D. Johnsonbaugh, T.J. Beveridge, Characterization of the binding of gallium, platinum, and uranium to *Pseudomonas fluorescens* by small-angle X-ray scattering and transmission electron microscopy, Appl. Environ. Microbiol. 59 (1993) 4056–4064.